REMARKS

A. Status of the Claims

Claim 3 has been canceled, and claims 1-2, 4-31 are pending, of which claims 11-23 and 26-30 are withdrawn. Claims 1, 4 and 6 have been amended. Thus, claims 1-2, 4-10, 24-25 and 31 are pending and under examination. No new matter has been added. Support for the amendment to claim 1 can be found at least in original, now-canceled claim 3.

B. Claim Objections

Applicants respectfully traverse the objection as to claims 24 and 25, noting that the non-elected claims are still pending.

C. Section 112, Second Paragraph Rejections

With respect to the "human or mouse" issue, Applicants have amended claim 6 in a manner that is believed to address the Examiner's concerns.

With respect to the term "stringent hybridization conditions," Applicants note that this term is well known in the art, as evidenced by the enclosed excerpt from the Sambrook laboratory manual.

D. Section 112, First Paragraph Rejection

The Action maintains the rejection of all of the claims under examination, taking the position that the subject matter of these claims is not fully enabled:

(i) for 7-transmembrane receptors such as proto-oncogenes and

(ii) for such G-protein coupled receptors labelled in the first cellular loop and the carboxy-terminus.

In response, Applicants would first note that the claims have been amended and are now specifically directed to G-protein coupled receptors. With respect to the "first cellular loop"

labeling issue, Applicants previously presented evidence supporting enablement in this regard. However, the Examiner appeared to disregard this evidence on the basis of the Examiner's statement that the relevant figure in question, Figure J, was not included in the response. Applicants' counsel contacted the Examiner requesting permission to respond to final and provide the allegedly missing figure. The Examiner agreed to consider Figure J after final and to make it of record.

To assist the Examiner in understanding the relevance of Figure J, Applicants further enclose a declaration of one of the inventors, Carsten Hoffman, who provides a description of Figure J that is essentially the same and the description provided in response to the previous office action, but placed in the form of a declaration for evidentiary purposes.

As can be seen from the enclosed declaration of Carsten Hoffman, he first states that the present application convincingly demonstrates that prominent members of 7-transmembrane receptors, "namely the α_{2A}–adrenergic (neurotransmitter) receptor, the (adenosine) A2A-receptor and the parathyroid hormone (PTH hormone) receptors" (see, *e.g.*, page 7, bottom, of the specification), can indeed successfully be employed in accordance with the present invention (*e.g.* in the context of a reliable, fast an easy measurement of the activation of 7-transmembrane proteins"; see page 6 and 7 bridging paragraph, of the specification).

He continues by stating that this evidence makes it clear that the present application provides evidence that 7-transmembrane receptors can generally be employed successfully in accordance with the teaching of the present application. Further evidence of enablement can be found in the fact that we have shown that a FRET-fluorophore does not negatively affect the receptor function, even if it is inserted into the <u>first</u> intracellular loop (see, *e.g.*, Fig. J, attached

hereto). Thus, he concludes, there is no basis for questioning that the introduction of FRET-fluorophores into other 7-transmembrane receptors will negatively effect their function.

With respect to Figure J, Carsten Hoffman states that this figure shows the effects of agonists on the FRET-response of the alpha2A receptor. Relative fluorescence intensity ratio was calculated from fluorescence emission measured at 480nm and at 530nm from cells expressing the receptor sensor and super-fused for the indicated period of time with the agonist nor-epinephrine (NE). The alpha2A receptor was labelled with CFP (donor fluorophore) at the C-terminus and FlAsH (acceptor fluorophore) within the first intracellular loop.

Mr. Hoffmann continues by noting that Figure J shows that receptor constructs can actually be generated also with labels inserted within the first intracellular loop, proving that functional receptor constructs in accordance with the entire breadth of claim 1 can be achieved. This is irrespective of the biological downstream function of the receptor, for example with respect to G-protein-coupling. He states that functional G protein-coupling is not necessary to allow the receptor constructs to respond according to the invention in a receptor FRET assay. Therefore, he concludes that the Examiner's argument against loop 1 or loop 3 constructs at the end of page 5 turn to 6 disturbing G protein-coupling is plainly invalid. He then states that his group has shown in several publications (for example Vilardaga *et al.*, *Nature Biotechnology* 2003, Hoffmann *et al.*, *Nature Methods* 2005; both enclosed) that receptors with altered G protein-coupling does still respond as FRET-sensors in accordance with the teaching of the present invention.

Mr. Hoffman continues by explaining Figures A-H, which provide examples of labeling at the C-terminus and third loop. Here he states that in order to support the above line of argument that the examples provided in the present application can be generalized to basically all

G-protein-coupled 7-transmembrane receptors, he provides examples of further 7-transmembrane receptors which have successfully been used in accordance with the present invention. These further examples of G protein coupled receptors are (Figures attached):

(a) the human M1-muscarinic receptor (Figure A and B),

(b) the human M3-muscarinic receptor (Figure C and D),

(c) the human M5-muscarinic receptor (Figure E) and

(d) the human H1-histamine receptor (Figure G and H).

Mr. Hoffman continues by noting that each of the foregoing were labelled at the third intracellular loop and the C-terminus with the combination of FlAsH and CFP. Figures A, C, E and G display the ratio between the CFP and FlAsH fluorescence, whereas Figures B, D and H display the CFP and FlAsH traces separately. Figure F displays the concentration-effect relationship for the M1, 3 and 5 muscarinic receptors which further underscores the utility of the recombinant G protein coupled constructs of the present invention. All of the above exemplified further 7-transmembrane receptors have already been mentioned in the application as originally filed (see, e.g., page 40 of the specification, middle of the page) and belong to the group of G-protein-coupled receptors.

Mr. Hoffman concludes by submitting that the foregoing provides strong evidence that the teachings of the present invention are broadly applicable to G protein coupled receptors in general, and that it is evident that Figure J provides supporting data that also the first intracellular loop can be labelled in order to create functional G protein coupled receptor constructs in accordance with the present invention.

Applicants submit that by the foregoing evidence the presently claimed invention has been shown to be fully enabled.

CONCLUSION

Applicants believe that the foregoing remarks fully respond to all outstanding matters for this application. Applicants respectfully request that the rejections of all claims be withdrawn so they may pass to issuance.

Should the Examiner desire to sustain any of the rejections discussed in relation to this Response, the courtesy of a telephonic conference between the Examiner, the Examiner's supervisor, and the undersigned attorney at 512-536-3055 is respectfully requested.

Respectfully submitted,

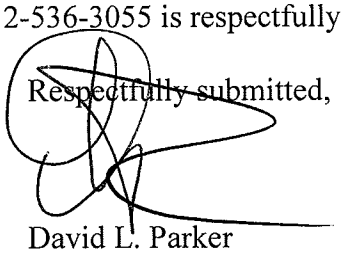

David L. Parker
Reg. No. 32,165
Attorney for Applicants

FULBRIGHT & JAWORSKI L.L.P.
600 Congress Avenue, Suite 2400
Austin, Texas 78701
(512) 474-5201
(512) 536-4598 (facsimile)

Date: January 22, 2010

Hybridization of Radiolabeled Probes to Nucleic Acids Immobilized on Nitrocellulose Filters or Nylon Membranes

Although the method given below deals with RNA or DNA immobilized on nitrocellulose filters, only slight modifications are required to adapt the procedure to nylon membranes. These modifications are noted at the appropriate places in the text.

1. Prepare the prehybridization solution appropriate for the task at hand. Approximately 0.2 ml of prehybridization solution will be required for each square centimeter of nitrocellulose filter or nylon membrane.

   The prehybridization solution should be filtered through a 0.45-micron disposable cellulose acetate filter (Schleicher and Schuell Uniflow syringe filter No. 57240 or equivalent).

Prehybridization solutions

For detection of low-abundance sequences:

Either
6× SSC (or 6× SSPE)
5× Denhardt's reagent
0.5% SDS
100 μg/ml denatured, fragmented salmon sperm DNA

or
6× SSC (or 6× SSPE)
5× Denhardt's reagent
0.5% SDS
100 μg/ml denatured, fragmented salmon sperm DNA
50% formamide

For preparation of Denhardt's reagent and denatured, fragmented salmon sperm DNA, see Table 9.1.

Formamide: Many batches of reagent-grade formamide are sufficiently pure to be used without further treatment. However, if any yellow color is present, the formamide should be deionized by stirring on a magnetic stirrer with Dowex XG8 mixed-bed resin for 1 hour and filtering twice through Whatman No. 1 paper. Deionized formamide should be stored in small aliquots under nitrogen at −70°C.

For detection of moderate- or high-abundance sequences:

Either
6× SSC (or 6× SSPE)
0.05× BLOTTO

or
6× SSC (or 6× SSPE)
0.05× BLOTTO
50% formamide

For preparation of BLOTTO, see Table 9.1.

When ^{32}P-labeled cDNA or RNA is used as a probe, poly(A)$^+$ RNA at a concentration of 1 μg/ml may be included in the prehybridization and hybridization solutions to prevent the probe from binding to T-rich sequences that are found fairly commonly in eukaryotic DNA.

2. Float the nitrocellulose filter or nylon membrane containing the target DNA on the surface of a tray of 6 × SSC (or 6 × SSPE) until it becomes thoroughly wetted from beneath. Submerge the filter for 2 minutes.

3. Slip the wet filter into a heat-sealable bag (e.g., Sears Seal-A-Meal or equivalent). Add 0.2 ml of prehybridization solution for each square centimeter of nitrocellulose filter or nylon membrane.

   Squeeze as much air as possible from the bag. Seal the open end of the bag with the heat sealer. Incubate the bag for 1–2 hours submerged at the appropriate temperature (68°C for aqueous solvents; 42°C for solvents containing 50% formamide).

   Often, small bubbles of air form on the surface of the filter as the temperature of the prehybridization solution increases. It is important that these bubbles be removed by occasionally agitating the fluid in the bag; otherwise, the components of the prehybridization solution will not be able to coat the filter evenly. This problem can be minimized by heating the prehybridization solution to the appropriate temperature before adding it to the bag.

4. If the radiolabeled probe is double-stranded, denature it by heating for 5 minutes at 100°C. Single-stranded probe need not be denatured. Chill the probe rapidly in ice water.

   Alternatively, the probe may be denatured by adding 0.1 volume of 3 N NaOH. After 5 minutes at room temperature, transfer the probe to ice water and add 0.05 volume of 1 M Tris · Cl (pH 7.2) and 0.1 volume of 3 N HCl. Store the probe in ice water until it is needed.

   For Southern hybridization of mammalian genomic DNA where each lane of the gel contains 10 μg of DNA, 10–20 ng/ml radiolabeled probe (sp. act. = 10^9 cpm/μg or greater) should be used. For Southern hybridization of fragments of cloned DNA where each band of the restriction digest contains 10 ng of DNA or more, much less probe is required. Typically, hybridization is carried out for 6–8 hours using 1–2 ng/ml radiolabeled probe (sp. act. = 10^9 cpm/μg or greater).

5. Working quickly, remove the bag containing the filter from the water bath. Open the bag by cutting off one corner with scissors. Add the denatured probe to the prehybridization solution, and then squeeze as much air as possible from the bag. Reseal the bag with the heat sealer so that as few bubbles as possible are trapped in the bag. To avoid radioactive contamination of the water bath, the resealed bag should be sealed inside a second, noncontaminated bag.

   When using nylon membranes, the prehybridization solution should be *completely* removed from the bag and immediately replaced with hybridization solution. The probe is then added and the bag is resealed.

Hybridization solution for nylon membranes

6× SSC (or 6× SSPE)
0.5% SDS
100 μg/ml denatured, fragmented salmon sperm DNA
50% formamide (if hybridization is to be carried out at 42°C)

6. Incubate the bag submerged in a water bath set at the appropriate temperature for the required period of hybridization.

7. Wearing gloves, remove the bag from the water bath and immediately cut off one corner. Pour out the hybridization solution into a container suitable for disposal, and then cut the bag along the length of three sides. Remove the filter and immediately submerge it in a tray containing several hundred milliliters of 2× SSC and 0.5% SDS at room temperature.

   Important: Do not allow the filter to dry out at any stage during the washing procedure.

8. After 5 minutes, transfer the filter to a fresh tray containing several hundred milliliters of 2× SSC and 0.1% SDS and incubate for 15 minutes at room temperature with occasional gentle agitation.

   If short oligonucleotides are used as probes, washing should be carried out only for brief periods (1–2 minutes) at the appropriate temperature. For a discussion of the stability of hybrids involving oligonucleotides, see Chapter 11.

9. Transfer the filter to a flat-bottom plastic box containing several hundred milliliters of fresh 0.1× SSC and 0.5% SDS. Incubate the filter for 30 minutes to 1 hour at 37°C with gentle agitation.

10. Replace the solution with fresh 0.1× SSC and 0.5% SDS, and transfer the box to a water bath set at 68°C for an equal period of time. Monitor the amount of radioactivity on the filter using a hand-held minimonitor. The parts of the filter that do not contain DNA should not emit a detectable signal. You should not expect to pick up a signal on the minimonitor from filters containing mammalian DNA that has been hybridized to single-copy probes.

11. Briefly wash the filter with 0.1× SSC at room temperature. Remove most of the liquid from the filter by placing it on a pad of paper towels.

12. Place the damp filter on a sheet of Saran Wrap. Apply adhesive dot labels marked with radioactive ink to several asymmetric locations on the Saran Wrap. These markers serve to align the autoradiograph with the filter. Cover the labels with Scotch Tape. This prevents contamination of the film holder or intensifying screen with the radioactive ink.

    Radioactive ink is made by mixing a small amount of ^{32}P with waterproof black drawing ink. We find it convenient to make the ink in three grades: very hot

(>2000 cps on a hand-held minimonitor), hot (>500 cps on a hand-held minimonitor), and cool (>50 cps on a hand-held minimonitor). Use a fiber-tip pen to apply ink of the desired hotness to the adhesive labels. Attach radioactive-warning tape to the pen, and store it in an appropriate place.

13. Cover the filter with a second sheet of Saran Wrap, and expose the filter to X-ray film (Kodak XAR-2 or equivalent) to obtain an autoradiographic image (see Appendix E). The exposure time should be determined empirically. However, single-copy sequences in mammalian genomic DNA can usually be detected after 16–24 hours of exposure at −70°C with an intensifying screen.

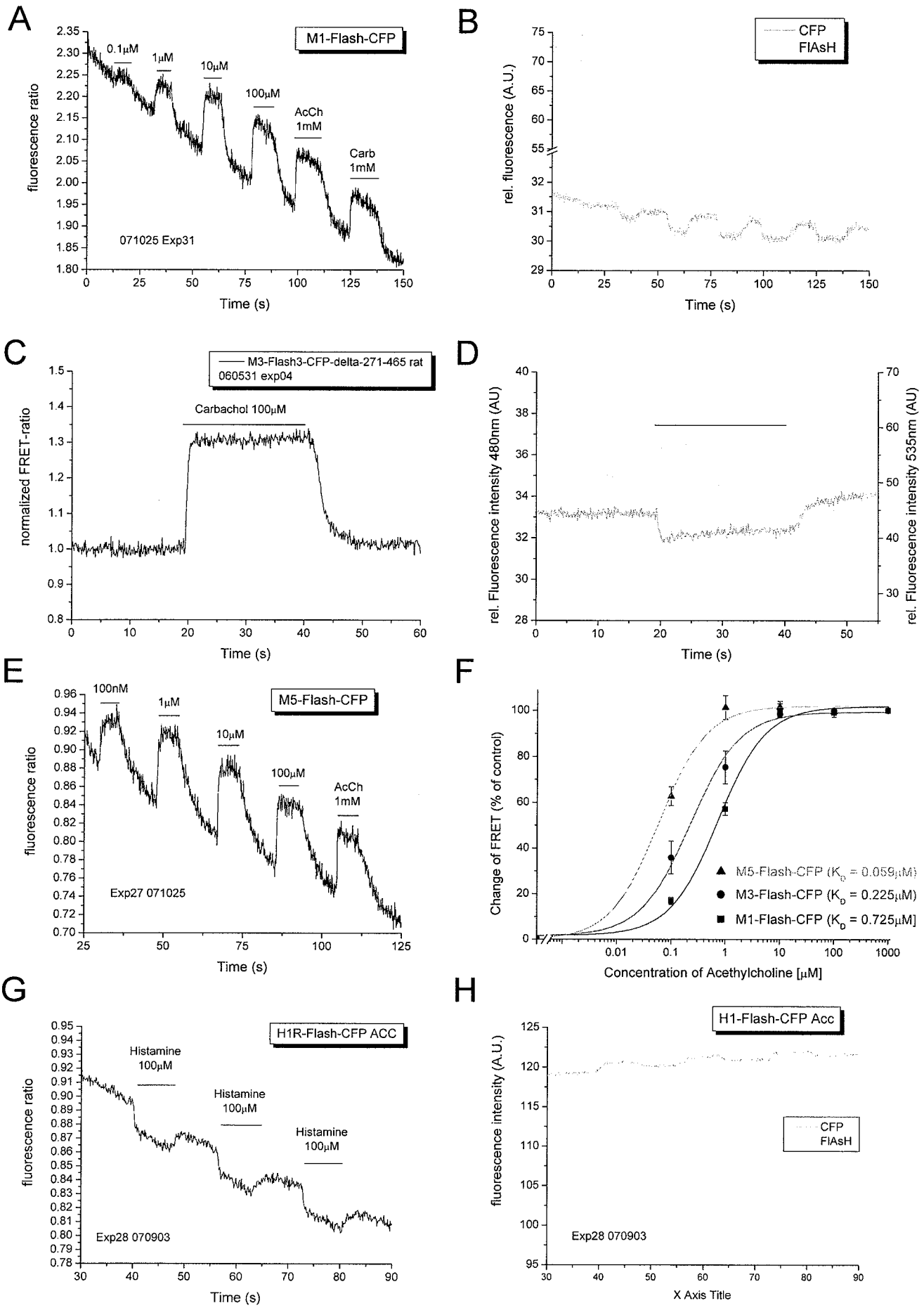
A
M1-Flash-CFP
0.1μM
1μM
10μM
100μM
AcCh 1mM
Carb 1mM
071025 Exp31
fluorescence ratio
Time (s)
B
CFP
FlAsH
rel. fluorescence (A.U.)
Time (s)
C
M3-Flash3-CFP-delta-271-465 rat 060531 exp04
Carbachol 100μM
normalized FRET-ratio
Time (s)
D
rel. Fluorescence intensity 480nm (AU)
rel. Fluorescence intensity 535nm (AU)
Time (s)
E
M5-Flash-CFP
100nM
1μM
10μM
100μM
AcCh 1mM
Exp27 071025
fluorescence ratio
Time (s)
F
Change of FRET (% of control)
M5-Flash-CFP (K_D = 0.059μM)
M3-Flash-CFP (K_D = 0.225μM)
M1-Flash-CFP (K_D = 0.725μM)
Concentration of Acethylcholine [μM]
G
H1R-Flash-CFP ACC
Histamine 100μM
Histamine 100μM
Histamine 100μM
Exp28 070903
fluorescence ratio
Time (s)
H
H1-Flash-CFP Acc
CFP
FlAsH
Exp28 070903
fluorescence intensity (A.U.)
X Axis Title

J

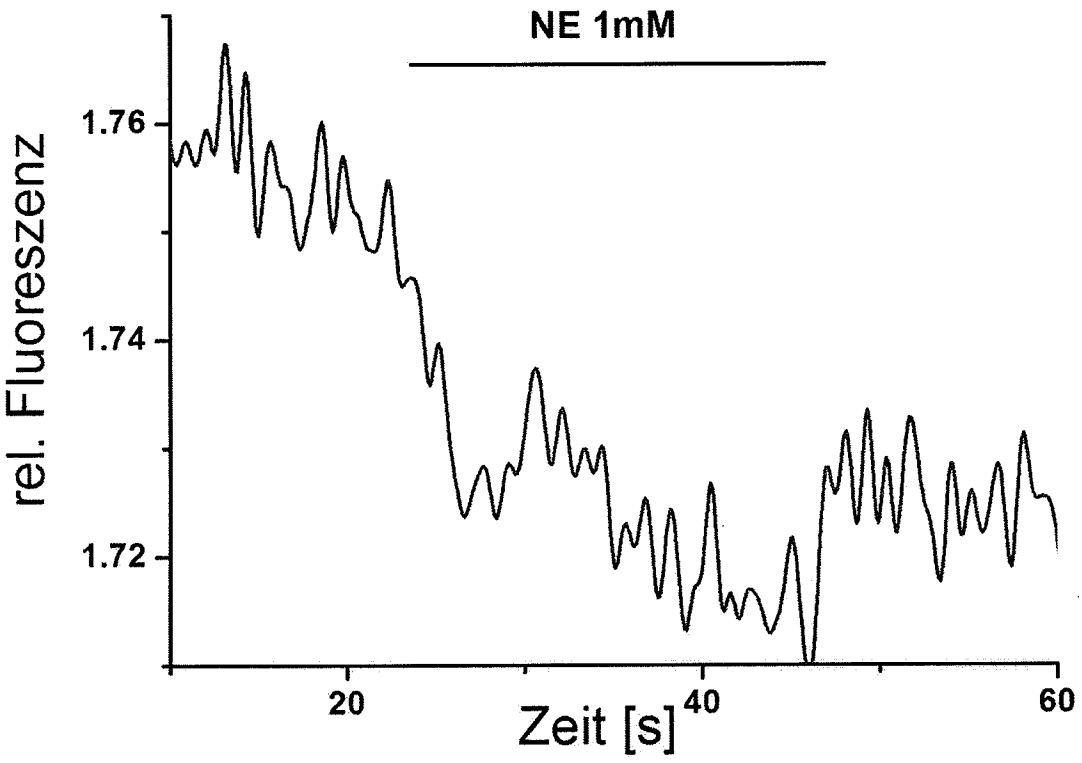

nature biotechnology

Measurement of the millisecond activation switch of G protein–coupled receptors in living cells

Jean-Pierre Vilardaga[1,2], Moritz Bünemann[1,2], Cornelius Krasel[1], Mariàn Castro[1] & Martin J Lohse[1]

Hormones and neurotransmitters transduce signals through G protein–coupled receptors (GPCR). Despite their common signaling pathways, however, the responses they elicit have different temporal patterns. To reveal the molecular basis for these differences we have developed a generally applicable fluorescence-based technique for real-time monitoring of the activation switch of GPCRs in living cells. We used such direct measurements to investigate the activation of the α_{2A}-adrenergic receptor (α_{2A}AR; neurotransmitter) and the parathyroid hormone receptor (PTHR; hormone) and observed much faster kinetics than expected: ~40 ms for the α_{2A}AR and ~1 s for the PTHR. The different switch times are in agreement with the different receptors' biological functions. Agonists and antagonists could rapidly switch the receptors on or off, whereas a partial agonist caused only a partial signal. This approach allows the comparison of agonist and partial agonist intrinsic activities at the receptor level and provides evidence for millisecond activation times of GPCRs.

G protein–coupled receptors constitute the largest family of hormone or neurotransmitter receptors and exhibit a common structure containing seven transmembrane α-helices[1–3]. Their activation by specific agonists—hormones or neurotransmitters—elicits a switch into an active state that binds to and thereby activates G proteins, the signal transducers. The G proteins, in turn, can activate a multitude of effector proteins such as ion channels or second messenger–producing enzymes that alter many functions in virtually every cell type including cardiovascular, neural and endocrine. A large body of data suggests that agonist-induced activation leads to a relative rearrangement of the receptor's transmembrane helices, most notably of helices III and VI (refs. 4–8).

A special case of a GPCR is rhodopsin, a receptor that senses light by using a covalently coupled ligand, 11-*cis* retinal, which isomerizes upon capture of a photon. In this case, conformational changes in the rhodopsin can be inferred from spectroscopic studies of the bound retinal, and multiple activation states formed within milliseconds have been detected[4,9]. No comparable approach is available for hormone- or transmitter-activated receptors. Spectroscopic studies have been done with purified β_2-adrenergic receptors chemically labeled with fluorophores and reconstituted into lipid membranes[10–13]. These studies observed agonist-mediated fluorescence changes on a time scale of minutes. This is much slower than the biological response to receptor activation, which can occur within seconds. To overcome this limitation, we devised a fluorescence approach that allows observation of the conformational switch of receptor activation *in vivo* at high temporal resolution.

We used two models of GPCRs: the PTHR, which is a member of the class 2 GPCRs[14] and binds the large hormone PTH (MW ~3,700), and the α_{2A}AR, which is a class 1 GPCR[14] and binds noradrenaline, a small (MW= 169) neurotransmitter. The PTHR transmits its signals to the G proteins G_s and G_q, and thereby causes increases in the second messengers cAMP and inositol trisphosphate; the α_{2A}AR couples to G_i and G_o and thereby decreases cAMP and regulates N-type Ca^{2+} and G protein–activated inwardly rectifying K^+ (GIRK) channels. Because it is thought that activation of receptors including the PTHR involves a change in the relative positions of the cytoplasmic parts of transmembrane helices III and VI (refs. 6, 15), we reasoned that a movement of helix VI should be transmitted to the third intracellular loop of the receptor.

To monitor such movements, we generated a series of receptor mutants into which the cyan- and yellow-emitting variants of the green fluorescent protein (CFP and YFP; reviewed in refs. 16, 17) were inserted at various positions of the third intracellular loop and/or of the C terminus of the two receptors, respectively. We report here the generation of such mutants and their use to monitor receptor activation.

RESULTS

Generation of receptor constructs with agonist-sensitive FRET

A series of receptor constructs were generated carrying CFP or YFP, or both, in various positions of the third intracellular loop or the C terminus of the PTHR and the α_{2A}AR, respectively. All of these constructs retained the essential binding and signaling properties of their parent receptors (see later). The two constructs showing the best agonist sensitivity by fluorescence resonance energy transfer (FRET) were used in this study and are referred to as receptor cameleons PTHR-cam and α_{2A}AR-cam (Fig. 1a).

Emission fluorescence spectra were recorded from HEK293 cells stably expressing PTHR-cam and various control constructs. Excitation of a PTHR carrying only a CFP moiety in its third intracellular loop (PTHR-$CFP_{3\text{-loop}}$) with light at 436 nm resulted in an emission at 480 nm (corresponding to the CFP emission, Fig. 1b). The additional presence of YFP in the C terminus (PTHR-cam) led

[1]Institute of Pharmacology and Toxicology, University of Würzburg, Versbacher Str. 9, D-97078 Würzburg, Germany. [2]These authors contributed equally to this work. Correspondence should be addressed to M.J.L. (lohse@toxi.uni-wuerzburg.de).

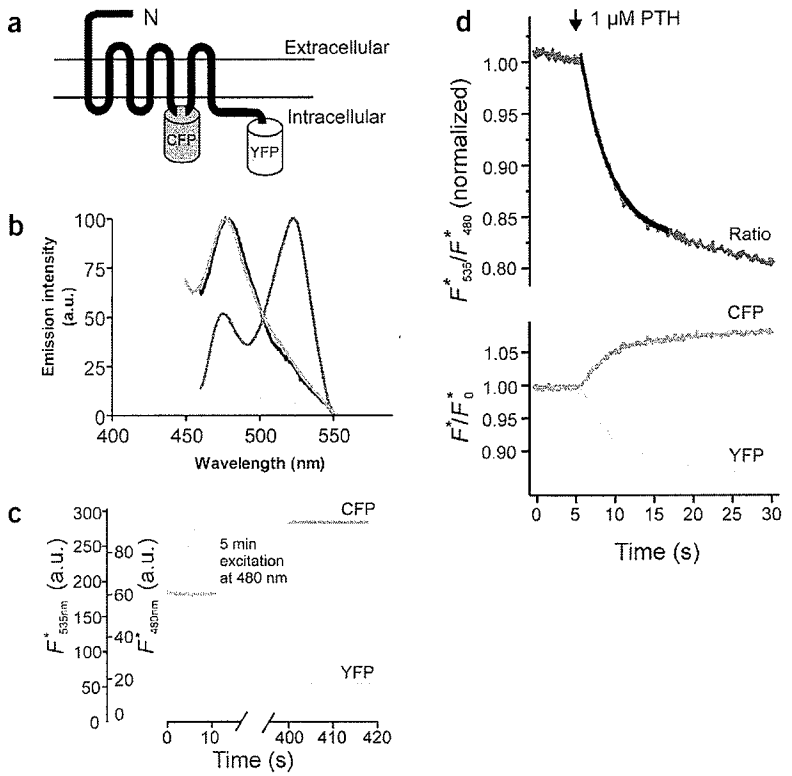

Figure 1 FRET efficiency and time-resolved changes in the FRET signal of PTHR-cam. (**a**) Overall transmembrane topology of the GPCR-cam constructs. (**b**) Fluorescence emission spectra of selected PTHR constructs. Shown are the emission spectra of PTHR-$CFP_{3\text{-loop}}$ (blue), PTHR-$YFP_{C\text{-term}}$ (yellow), simultaneous PTHR-$CFP_{3\text{-loop}}$ + PTHR-$YFP_{C\text{-term}}$ (black), and PTHR-cam (red) upon excitation at 433 nm. (**c**) Effect of photobleaching. Emission intensities of YFP (535 nm, yellow) and CFP (480 nm, blue) were recorded simultaneously from single cells expressing PTHR-cam using fluorescence microscopy. Emission intensities were recorded before and after the acceptor fluorophore was photobleached by 5 min exposure to light at 480 nm. (**d**) Time-resolved changes in the ratio F^*_{535}/F^*_{480} in single HEK293 cells stably expressing PTHR-cam. Emission intensities of YFP (535 nm, yellow), CFP (480 nm, blue) and the ratio F^*_{535}/F^*_{480} (red) were recorded simultaneously from single cells. Shown are the changes induced by rapid superfusion with 1 μM PTH (arrow). The decrease of the ratio F^*_{535}/F^*_{480} was fitted by a simple monoexponential curve giving a time constant in this experiment of 3.5 s. Changes in the ratio are expressed as percentage decrease from the initial value at $t = 0$ s.

to reduced emission at 480 nm and a strong emission at the characteristic wavelength of YFP (535 nm, Fig. 1b). Photobleaching of the acceptor confirmed that the latter emission was primarily due to FRET (see Fig. 1c). The presence of YFP in the C terminus alone (PTHR-$YFP_{C\text{-term}}$) or coexpression of PTHR-$CFP_{3\text{-loop}}$ and PTHR-$YFP_{C\text{-term}}$ did not result in marked emission at 535 nm when excited at 436 nm (Fig. 1b).

Signals recorded from single HEK293 cells expressing PTHR-cam were then analyzed at emissions of 480 nm (CFP) and 535 nm (YFP) upon excitation at 436 nm (CFP excitation). The microscopic illumination allowed photobleaching experiments to verify that the emission at 535 nm was indeed due to FRET. After bleaching of the acceptor in the PTHR-cam construct with intense light at 480 nm, the emission at 480 nm increased by 50 ± 3% together with a reduction of the 535 nm emission of more than fivefold (Fig. 1c). Similar spectral and photobleaching data were obtained with the α_{2A}AR-cam stably expressed in HEK293 cells (data not shown).

We then investigated the effects of the agonist PTH on the FRET signal of PTHR-cam, measured as the bleedthrough-corrected emission intensity ratio F^*_{535}/F^*_{480}. After addition of 1 μM PTH, the ratio F^*_{535}/F^*_{480} rapidly decreased (Fig. 1d). After a short delay (~600 ms), the decrease followed a monoexponential time course with a time constant $\tau = 3.00 \pm 0.25$ s ($n = 9$). The symmetrical increase in CFP emission and decrease in YFP emission indicate that the change was due to a decrease in FRET. Control experiments with coexpression of PTHR-$CFP_{3\text{-loop}}$ and PTHR-$YFP_{C\text{-term}}$ showed no FRET in the absence or in the presence of PTH (1 μM) and thus made it unlikely that the signals resulted from intermolecular FRET in receptor dimers (Fig. 1b). It should be noted, however, that the intramolecular nature of this signal does not exclude the presence of receptor dimers.

Similarly, α_{2A}AR-cam showed intramolecular FRET, and again the specific agonist (noradrenaline) caused a decline of the FRET signal (see later). Virtually identical results were obtained with the two receptors expressed in Chinese hamster ovary (CHO) and neuronal PC12 cells (data not shown). The agonist-induced decreases in FRET in the two types of receptors suggest that the agonist-induced conformational switch is similar in class 1 and class 2 GPCRs. Because of the location of the CFP and YFP in the receptors (Fig. 1a), the FRET signals are compatible with a movement of the third intracellular loop away from the C terminus as predicted by computer simulations of the α_{1B}-adrenergic receptor[18].

Pharmacological characterization of the receptor-cameleon

The receptor-cameleon constructs stably expressed in HEK293 cells retained the typical ligand binding, which was of somewhat lower affinity than for the corresponding wild-type receptors (Fig. 2): the PTH affinity was $K_i = 15.5 \pm 0.9$ nM for PTHR-cam and $K_i = 2.4 \pm 0.4$ nM for PTHR; the noradrenaline affinity was $K_i = 5.0 \pm 0.8$ μM for α_{2A}AR and $K_i = 16.7 \pm 1.4$ μM for α_{2A}AR-cam. Note that the insertion of the GFP variants into the third loop and C terminus of the receptor might cause a conformational destabilization of the receptor, resulting in a deviation in the binding properties of the GPCRs-cam. Such destabilization might result in a faster activation switch of the receptor. However, the α_{2A}AR-cam-induced GIRK current activation was no faster than that caused by the wild-type α_{2A}AR (data not shown, and ref. 19).

PTHR-cam and α_{2A}AR-cam signaled efficiently to adenylyl cyclase (half-maximal effective concentration, $EC_{50} = 12.8 \pm 1.4$ nM) and to the GIRK channel ($EC_{50} = 1.08 \pm 0.01$ μM), respectively (Fig. 2a,b). A difference in the signal amplification between PTHR wild-type- and PTHR-cam receptors (1 μM PTH mediated a 28- versus an 11.5-fold increase in cAMP in HEK293 cells stably expressing PTHR or PTHR-cam, respectively) is in part due to the higher expression level of the wild-type receptors (1.01×10^6 versus 0.34×10^6 receptors/cell for PTHR and PTHR-cam, respectively). The entire series of receptor-cameleon constructs that we generated had signaling properties very

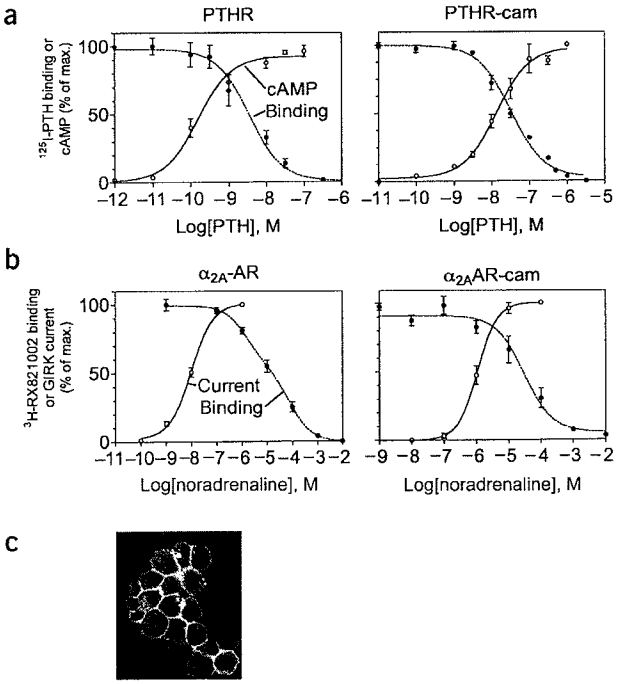

Figure 2 Pharmacological properties of the GPCR-cam constructs. (**a**, **b**) Comparison between the binding and signaling properties of PTHR-cam, α_{2A}AR-cam and their respective wild-type receptor stably expressed in HEK293 cells. The expression of the receptors was 1.01×10^6 and 0.34×10^6 receptors/cells for PTHR and PTHR-cam, respectively; 24 and 6 pmol/mg for α_{2A}AR and α_{2A}AR-cam, respectively. The data are the means ± s.e. of at least four separate experiments carried out in duplicate. (**c**) Visualization of stably expressed PTHR-cam in HEK293 cells by confocal microscopy.

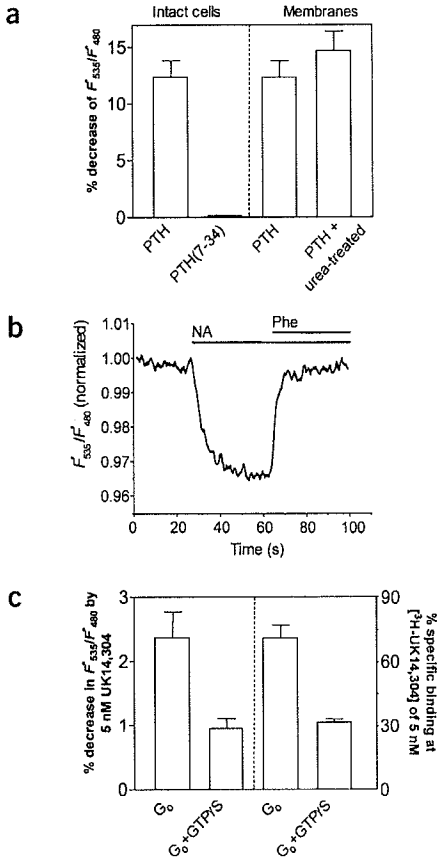

Figure 3 Agonist-induced decrease in FRET signal corresponds to receptor activation. (**a**) Intact cells panel shows the effects of the agonist PTH (1 μM) and the antagonist PTH(7-34) (3 μM) on the ratio F^*_{535}/F^*_{480} of PTHR-cam in intact HEK293 cells. Membranes panel shows the effects of PTH (1 μM) in cell membranes prepared from HEK293 cells stably expressing PTHR-cam. The membranes were measured either without further treatment (left) or after treatment with 6 M urea (right). Bars represent the percentage decrease in the ratio F^*_{535}/F^*_{480} upon PTH exposure. (**b**) Effect of the antagonist phentolamine (Phe; 10 μM) on the FRET signal caused by 10 μM noradrenaline (NA) in HEK293 cells stably expressing α_{2A}AR-cam ($n = 4$). (**c**) Comparison of the guanine nucleotide sensitivity of the FRET signal (left panel) and agonist binding (right panel) evoked by a subsaturating concentration of UK14304 (5 nM) in membranes containing α_{2A}AR-cam in the presence of G_o proteins (ratio of receptor to G_o = 1:100) with or without GTPγS (10 μM). Data are the means ± s.e. of at least four separate experiments.

similar to those of PTHR-cam (data not shown). Finally, confocal microscopy showed that the majority of PTHR-cam (Fig. 2c) and α_{2A}AR-cam receptors (not shown) in stably transfected cells were present at the cell surface. These data indicate that both receptor constructs were properly targeted to the cell surface upon expression in HEK293 cells and retained essential binding properties as well as significant G protein–mediated signaling of the corresponding wild-type receptors. Similar data were obtained upon expression in various cell lines including CHO and neuronal PC12 cells (data not shown).

Agonist-mediated FRET reflects receptor activation

How can we be sure that the agonist-induced changes in FRET do indeed reflect the conformational change of the receptor? We sought to answer this critical question along several lines.

First, we set out to prove that the FRET signal was indeed caused by the receptors themselves and not by interactions with other proteins such as G proteins or β-arrestins. To this end, we studied PTHR-cam under conditions that exclude interactions with these proteins. In isolated cell membranes prepared from HEK293 cells stably expressing PTHR-cam (that is, in the absence of cytosolic proteins), the PTH-induced signal had the same magnitude as in intact cells (Fig. 3a). Further stripping the cell membranes with 6 M urea—a treatment known to leave GPCRs intact but to denature virtually all other proteins[6,20]—did also not affect the magnitude of the PTH-induced signal at saturating concentrations (Fig. 3a). Finally, inactivating G_i and G_o with pertussis toxin in cells expressing the α_{2A}AR-cam did not affect the noradrenaline-induced FRET signal (data not shown), indicating that the signal was not due to a receptor–G protein interaction. Taken together, these data strongly suggest that the FRET signals were not caused by interactions of the receptors with other proteins.

Second, we wanted to prove that the FRET signals correspond to the activation state of the receptor. To do this, we investigated the effects of agonists and antagonists. A truncated variant of PTH, PTH7-34, which is a low-affinity antagonist, failed to induce a change in FRET (Fig. 3a). Similarly, noradrenaline (10 μM) induced a rapid decrease of the FRET signal in the α_{2A}AR-cam (Fig. 3b), whereas saturating concentrations of the high-affinity α_2-adrenergic receptor antagonist phentolamine (10 μM) did not alter the FRET signal when given alone

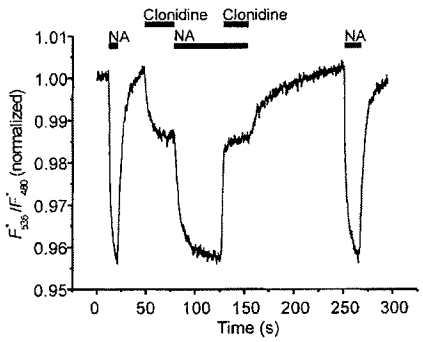

Figure 4 Action of the partial agonist clonidine on α_{2A}AR-cam. Changes in FRET in response to 10 μM noradrenaline (NA) or 10 μM clonidine added alone or together were recorded in a single HEK293 cell expressing α_{2A}AR-cam. The recording is representative of four independent experiments.

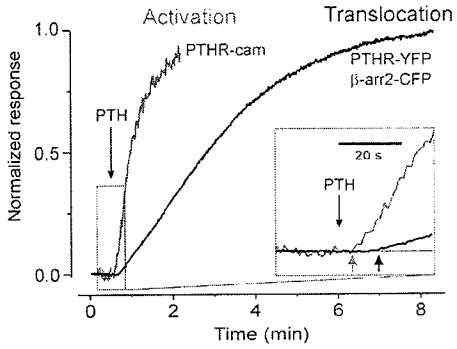

Figure 5 Comparison between the dynamics of receptor activation and desensitization of PTHR-cam. The kinetics of activation of PTHR-cam and of β-arrestin2-YFP binding to the PTHR-$CFP_{C\text{-}term}$ were measured as changes in the ratio F^*_{535}/F^*_{480} in single cells expressing PTHR-cam or coexpressing PTHR-$CFP_{C\text{-}term}$ and β-arrestin2-YFP in response to 100 nM PTH. The recordings are expressed as percentages of the respective maximal response and are representative of at least three independent experiments. Note that in the case of PTHR-$CFP_{C\text{-}term}$ and β-arrestin2-YFP the ratio F^*_{535}/F^*_{480} does indeed increase, whereas in the PTHR-cam the ratio decreases and is depicted as a positive signal just to facilitate the comparison of the kinetics. The inset represents a time scale expansion to illustrate the differences in response delays.

(not shown). However, phentolamine rapidly reverted the noradrenaline-induced signal (Fig. 3b). This is compatible with its nature as a competitive antagonist. Thus, the rigorous agonist dependence of the change of the FRET signal mirrors the active state of the receptor.

Third, binding of G proteins to receptors is known to enhance formation of the active, agonist-bound state. Because of the reduced ability of the receptor cameleons to couple to G proteins, such assays required the addition of exogenous G proteins. After addition of purified G_o to membranes containing α_{2A}AR-cam, the agonist ^{3}H-UK14304 bound with high affinity to the receptors (K_d = 3.4 ± 0.8 nM; see Supplementary Fig. 1 online). Addition of the stable GTP analog GTPγS reduced this affinity (K_d = 9.6 ± 1.1 nM), indicating a disruption of the high-affinity receptor–G protein complex. GTPγS reduced the binding of 5 nM ^{3}H-UK14304 by >50% (Fig. 3c, right panel). Similarly, GTPγS reduced the FRET signal caused by 5 nM UK14304 in the same membrane preparation (that is, in the presence of G_o) by >50% (Fig. 3c, left panel). GTPγS did not affect the signal at saturating concentrations of UK14304 (data not shown); this conforms with the lack of effect of urea treatment on the maximal PTH-induced signal obtained in membranes (Fig. 3a). Taken together, these data suggest that the FRET signal originates in the active conformation of the receptor itself, and that this active conformation binds to and is stabilized by G proteins.

FRET changes mediated by a partial agonist

The FRET assay also properly reflected partial agonism (Fig. 4). Compared with the full agonist noradrenaline, at saturating concentrations (10 μM) the high-affinity partial agonist clonidine resulted in a threefold smaller FRET signal (Fig. 4). Subsequent application of noradrenaline (10 μM) still induced the full response. The simultaneous addition of clonidine (10 μM) restored this response to the partial response seen with clonidine alone; and again, after washout, noradrenaline produced the full initial response. These data correspond exactly with the predicted properties of a high-affinity partial agonist. However, in comparison with other assays used to detect partial agonism, the FRET assay is not dependent on transducer and effector proteins but reflects the partial agonist effects on the receptors themselves. Mechanistically, the ability of clonidine to partially reverse the agonist-mediated signal suggests that the partial agonist restrains the complete movement between the third intracellular loop and the C terminus. This is compatible with the notion that the partial agonism process occurs at the receptor level by inducing a restrained conformational change within the agonist binding site[12].

Receptor activation precedes β-arrestin–receptor interaction

To show that receptor activation precedes receptor deactivation, we measured the onset of the association of β-arrestin with the receptor, the signal for PTHR deactivation[21,22]. To this end, we coexpressed functional PTHR carrying CFP at its C terminus (PTHR-$CFP_{C\text{-}term}$) and β-arrestin2 fused at its C terminus to YFP (β-arrestin2-YFP). We monitored PTH-induced binding of β-arrestin2 to the receptor by measuring the appearance of FRET between the CFP and the YFP. The dynamics of this signal were compared to the receptor activation of PTHR-cam (Fig. 5). The initial ratio F^*_{535}/F^*_{480} was 1.10 ± 0.05 for cells coexpressing PTHR-$CFP_{C\text{-}term}$ and β-arrestin2-YFP. After addition of PTH (100 nM), the ratio increased by up to 32 ± 11% with a $t_{1/2}$ of 150 ± 12.1 s (n = 8), reflecting the PTH-mediated receptor–β-arrestin2 association. The same concentration of PTH (100 nM) had a fivefold faster effect on PTHR-cam, with a $t_{1/2}$ of 32 ± 1.9 s (n = 4 experiments). Furthermore, the lag time between addition of PTH and the beginning of the response was about three times shorter for the activation signal (PTHR-cam) than for β-arrestin translocation (Fig. 5, inset). Similar results, but with a much lower amplitude, were obtained with a similar α_{2A}AR-$CFP_{C\text{-}term}$ construct; again, the activation signal was earlier and much faster than that resulting from the interaction with β-arrestin2-YFP (data not shown). The speed of β-arrestin interaction with the receptor could be modulated by varying the expression levels of β-arrestin and G protein–coupled receptor kinases (GRKs), but even under optimal condition it was always much slower than the activation signal (data not shown). Thus, the signal for receptor activation indeed begins earlier and proceeds much faster than that for receptor deactivation.

Differential speed of activation distinct receptors

Time-resolved determination of the FRET signals recorded from single cells after activation with various concentrations of PTH and noradrenaline, respectively, allowed the analysis of the switch kinetics (Fig. 6). Under all conditions, the decrease of the ratio F^*_{535}/F^*_{480} followed a monoexponential time course. Increasing concentrations of

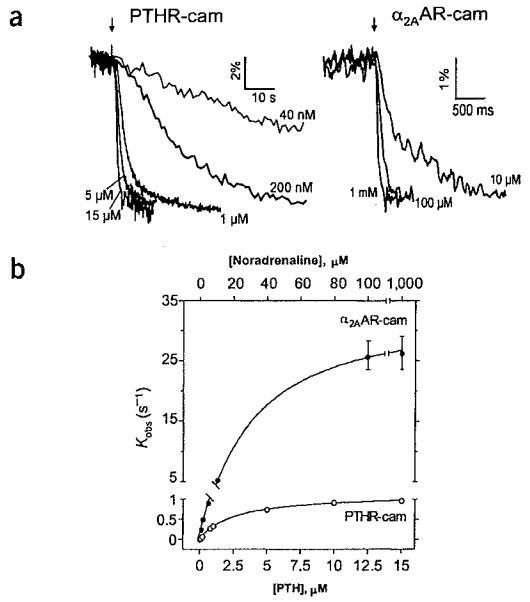

Figure 6 Dynamics of agonist-mediated receptor conformational change. (**a**) Time-resolved changes in the ratio F^*_{535}/F^*_{480} of the PTHR-cam (left panel) and α_{2A}AR-cam (right panel) expressed in HEK293 cells at various concentrations of PTH and noradrenaline, respectively. (**b**) Relationship between the apparent rate constant, k_{obs} and agonist concentration. k_{obs} values were obtained from fitting the kinetic data of **a** with a monoexponential equation. At low concentrations of agonist, k_{obs} values were directly proportional to the agonist concentration, whereas at higher concentrations of agonist the values approached a maximal value of ~1 s^{-1} and 26 s^{-1} for PTHR-cam and α_{2A}AR-cam, respectively. Note that the k_{obs} values depicted here saturate at much higher ligand concentrations than the binding data shown in **Figure 2**. This is because the k_{obs} values are not measured at equilibrium. Data indicate the mean ± s.e.m. of at least seven separate experiments.

agonist resulted in shorter delay times as well as faster time courses of the signals. At low agonist concentrations, the rate constants (k_{obs}) increased in proportion to agonist concentration (**Fig. 6b**), indicating that agonist binding to the receptors was the rate-limiting step. At higher concentrations of agonist, the rate constants reached a maximum, suggesting that a step other than the collisional probability of agonist-receptor became rate limiting. This limit is not due to technical constraints of the system, which allows complete solution exchange in <10 ms, but rather to the agonist-mediated conformational switch of the receptors. The time constant required for the receptor activation was <40 ms in the case of the α_{2A}AR-cam. This is much faster than the activation time measured for chemically labeled, purified β_2-adrenergic receptors[10–13] and corresponds well to the physiological requirements of neurotransmitter receptors. In contrast, the kinetics of the FRET signal were 25-fold slower ($\tau \approx 1$ s) for the PTHR.

DISCUSSION

The direct monitoring of ligand-induced FRET changes in GPCR-cam provided information about the activation switch of the receptor at the surface of living cells. The saturation of the k_{obs} values and the concentration-dependent delay times (**Fig. 6**) are compatible with a simple two-step process of first-order agonist binding and subsequent receptor activation. The delay times indicate that the FRET signal reflects the conformational switch underlying receptor activation and not just receptor-agonist contact. Mechanistically, this switch appears to be similar in class 1 and class 2 GPCRs, but the activation kinetics are much faster in the class 1 α_{2A}AR-cam. The slower activation of the class 2 PTHR is in agreement with the slow hormonal effect of PTH, compared with the fast synaptic action of noradrenaline. Millisecond switch times had been thus far thought to be limited to ion channel receptors[23] or to rhodopsin[9]. Our data indicate that a neurotransmitter GPCR can be switched in the millisecond time scale, and further show that the extent of switching is dependent on the intrinsic efficacy of the ligand.

In addition to providing an insight into the activation switch dynamics of GPCRs, receptor-cameleon constructs can also be applied to answer questions regarding the pharmacology of GPCRs, such as the effect of inverse agonists on receptor conformation, and aspects of receptor behavior, such as the spatiotemporal dynamics of receptor activation during neutrophil chemotaxis or the behavior of the β_1- and β_2-adrenergic receptor activity in cardiomyocytes.

METHODS

Molecular biology and cell culture. Site-directed mutagenesis was conducted on the human PTHR and the mouse α_{2A}AR cDNAs. The cDNAs encoding the enhanced YFP and CFP were fused to position Gly418 of the C terminus of the PTHR and inserted between Gly395 and Arg396 into the third intracellular loop of the PTHR, respectively. For the α_{2A}AR, YFP was inserted in the third intracellular loop between Ala250 and Ser371, and CFP was fused to Val461 in the C terminus. Constructions were achieved by PCRs as described[24]. β-arrestin2-YFP was assembled following the procedure described for the construction of β-arrestin1-GFP (ref. 25). Constructs were verified by sequencing. Receptor cDNAs were cloned into pCDNA3 (Invitrogen) for transient and stable expression in mammalian cells. HEK293, CHO and PC12 cells served as the expression systems for the wild-type and chimeric receptors. The procedure for the selection of stable cell lines has been described[15].

Pharmacology. Ligand binding, receptor number determination, cAMP assays, measurement of α_{2A}AR-activated GIRK currents and reconstitution of receptor-G_o coupling were measured as described[15,19,21,26]. Saturation and competition binding studies were analyzed with the program Prism to calculate K_d and K_i values.

Electrophysiology. Whole-cell GIRK currents were measured in HEK293 cells stably expressing 6 pmol/mg membrane protein α_{2A}AR-cam 20–28 h after transient transfection with GIRK1 and GIRK4 as described[19]. Membrane currents were recorded using an EPC 9 amplifier and Pulse software (HEKA Instruments) for voltage control, data acquisition and data evaluation. Experimental conditions such as patch pipettes, internal and external solutions, voltage-clamp protocol as well as the superfusion system were the same as described[19].

Fluorescence measurements. Cells were washed with PBS, scraped from the plate and resuspended in buffer A (137 mM NaCl, 5 mM KCl, 1 mM $CaCl_2$, 1 mM $MgCl_2$, 20 mM HEPES, 0.1% (wt/vol) BSA, pH 7.4) at a density of ~10^7 cells/ml. Steady-state fluorescence emission spectra of the cell suspension were measured with a spectrofluorometer (Perkin-Elmer) in cuvettes containing HEK293 cells expressing the indicated receptors, and were normalized to the respective maxima for PTHR-$CFP_{3\text{-loop}}$ and PTHR-cam. PTHR-$YFP_{C\text{-term}}$ was normalized relative to the maximal response upon exposure to 480 nm light.

FRET measurements. Cells grown on coverslips were maintained in buffer A at room temperature and placed on a Zeiss inverted microscope (Axiovert135) equipped with an oil immersion 63× objective and a dual-emission photometric system (Till Photonics). Samples were excited with light from a polychrome IV (Till Photonics). To minimize photobleaching, the illumination time was set to 5 ms applied with a frequency between 1 and 75 Hz dependent on agonist concentration. FRET was monitored as the emission ratio of YFP to CFP, F_{535}/F_{480}, where F_{535} and F_{480} are the emission intensities at 535 ± 15 nm and 480 ± 20 nm (beam splitter DCLP 505 nm) upon excitation at 436 ± 10 nm

(beam splitter DCLP 460 nm). The emission ratio was corrected by the respective spillover of CFP into the 535-nm channel (spillover of YFP into the 480-nm channel was negligible) to give a corrected ratio F^*_{535}/F^*_{480}. FRET between CFP and YFP in cells stably expressing the receptor constructs was also determined by donor recovery after acceptor bleaching. The increase in emission at 480 nm was 50 ± 3% after >80% bleaching of YFP (induced by 3–5 min continuous illumination with 480 ± 15 nm). To determine agonist-induced changes in FRET, cells were continuously superfused with buffer A and agonist was applied using a computer-assisted solenoid valve–controlled rapid superfusion device (ALA-VM8; ALA Scientific Instruments) (solution exchange 5–10 ms). Signals detected by avalanche photodiodes were digitalized using an AD converter (Digidata1322A; Axon Instruments) and stored on a personal computer using Clampex 8.1 software (Axon Instruments). The decrease in FRET ratio was fitted to the equation: $r(t) = A \times (1 - e^{-t/\tau})$, where τ is the time constant (s) and A is the magnitude of the signal. When necessary for calculating τ, agonist-independent changes in FRET due to photobleaching were subtracted.

Membrane preparation. Membrane fractions were obtained after two centrifugations at 4 °C, the first at 800 *g* for 10 min and the second at 100,000 *g* for 30 min. Membranes were treated with 6 M urea in 20 mM HEPES, pH 7.4, for 30 min on ice and then centrifuged at 100,000 *g* for 15 min. After two washing steps at 4 °C in 20 mM HEPES, pH 7.4, the membranes were resuspended in buffer A (without BSA) and immediately used in the experiments. Membranes were subjected to fluorescence microscopy in 20-µl aliquots similarly to intact cells using a 20× objective.

Note: Supplementary information is available on the Nature Biotechnology website.

ACKNOWLEDGMENTS

This paper is dedicated to R.J. Lefkowitz on the occasion of his 60th birthday. We thank Manfred Bernhard for support with the radioligand binding studies and Christian Dees for the G protein preparation. We are grateful to Martin Heck for help with computer simulations and Ernst J.M. Helmreich, Lutz Hein, Ursula Quitterer and Henry R. Bourne for critical comments on the manuscript. This work was supported by the Deutsche Forschungsgemeinschaft and the Fonds der Chemischen Industrie (grants to M.J.L.) and fellowships from the Alexander von Humboldt foundation and Ministerio de Ciencia y Tecnología, Spain (to M.C.).

COMPETING INTERESTS STATEMENT

The authors declare competing financial interests (see the *Nature Biotechnology* website for details).

Received 15 January; accepted 24 April 2003
Published online 15 June 2003; doi:10.1038/nbt838

1. Rohrer, D.K. & Kobilka, B.K. G protein–coupled receptors: functional and mechanistic insights through altered gene expression. *Physiol. Rev.* **78**, 35–52 (1998).
2. Gether, U. Uncovering molecular mechanisms involved in activation of G protein–coupled receptor. *Endocr. Rev.* **21**, 90–113 (2000).
3. Pierce, K., Premont, R.T. & Lefkowitz, R.J. Seven transmembrane receptors. *Nat. Rev. Mol. Cell Biol.* **3**, 639–650 (2002).
4. Farrens, D.L., Altenbach, C., Yang, K., Hubbell, W.L. & Khorana, H.G. Requirement of rigid-body motion of transmembrane helices for light activation of rhodopsin. *Science* **274**, 768–770 (1996).
5. Sheikh, S.P., Zvyaga, T.A., Lichtarge, O., Sakmar, T.P. & Bourne, H.R. Rhodopsin activation blocked by metal-ion-binding sites linking transmembrane helices C and F. *Nature* **383**, 347–350 (1996).
6. Sheikh, S.P. *et al.* Similar structures and shared switch mechanisms of the β_2-adrenoceptor and the parathyroid hormone receptor. *J. Biol. Chem.* **274**, 17033–17041 (1999).
7. Wieland, K., Zuurmond, H.M., Krasel, C., IJzerman, A.P. & Lohse, M.J. Involvement of Asn-293 in stereospecific agonist recognition and in activation of the β_2-adrenergic receptor. *Proc. Natl. Acad. Sci. USA* **93**, 9276–9281 (1996).
8. Ward, S.D.C., Hamdan, F.F., Bloodworth, L.M. & Wess, J. Conformational changes occur during M_3 muscarinic acetylcholine receptor activation probed by the use of an *in situ* disulfide cross-linking strategy. *J. Biol. Chem.* **277**, 2247–2257 (2002).
9. Okada, T., Ernst, O.P., Palczewski, K. & Hofmann, K.P. Activation of rhodopsin: new insights from structural and biochemical studies. *Trends Biochem. Sci.* **26**, 318–324 (2001).
10. Gether, U., Lin, S.B. & Kobilka, K. Fluorescent labeling of purified β_2-adrenergic receptor: evidence for ligand-specific conformational changes. *J. Biol. Chem.* **270**, 28268–28275 (1995).
11. Jensen, A.D. *et al.* Agonist-induced conformational changes at the cytoplasmic side of transmembrane segment 6 in the β_2-adrenergic receptor mapped by site-selective fluorescent labeling. *J. Biol. Chem.* **276**, 9279–9290 (2001).
12. Ghanouni, P. *et al.* Functionally different agonists induce distinct conformations in the G protein coupling domain of the β_2 adrenergic receptor. *J. Biol. Chem.* **276**, 24433–24436 (2001).
13. Ghanouni, J., Steenhuis, J., Farrens, D.L. & Kobilka, B.K. Agonist-induced conformational changes in the G-protein-coupling domain of the β_2 adrenergic receptor. *Proc. Natl. Acad. Sci. USA* **98**, 5997–6002 (2001).
14. Bockaert, J. & Pin, J.P. Molecular tinkering of G protein–coupled receptors: an evolutionary success. *EMBO J.* **18**, 1723–1729 (1999).
15. Vilardaga, J.P. *et al.* Differential conformational requirements for activation of G proteins and regulatory proteins, arrestin and GRK in the parathyroid hormone receptor. *J. Biol. Chem.* **276**, 33435–33443 (2001).
16. Tsien, R.Y. The green fluorescent protein. *Annu. Rev. Biochem.* **67**, 509–544 (1998).
17. Miyawaki, A. & Tsien, R.Y. Monitoring protein conformations and interactions by fluorescence resonance energy transfer between mutants of green fluorescent protein. *Methods Enzymol.* **327**, 472–501 (2000).
18. Greasley, P.J. *et al.* Mutational and computational analysis of the α_{1b}-adrenergic receptor. *J. Biol. Chem.* **276**, 46485–46494 (2001).
19. Bünemann, M., Bücheler, M.M., Philipp, M., Lohse, M.J. & Hein, L. Activation and deactivation kinetics of α_{2A}- and α_{2C}-adrenergic receptor–activated G protein–activated inwardly rectifying K^+ channel currents. *J. Biol. Chem.* **276**, 47512–47517 (2001).
20. Lim, W.J. & Neubig, R.R. Selective inactivation of guanine-nucleotide-binding regulatory protein (G-protein) α and βγ subunits by urea. *Biochem. J.* **354**, 337–344 (2001).
21. Vilardaga, J.P. *et al.* Internalization determinants of the parathyroid hormone receptor differentially regulates β-arrestin/receptor association. *J. Biol. Chem.* **277**, 8121–8129 (2002).
22. Castro, M. *et al.* Dual regulation of the parathyroid hormone (PTH)/PTH-related peptide receptor signaling by protein kinase C and β-arrestins. *Endocrinology* **143**, 3854–3865 (2002).
23. Chang, Y. & Weiss, D.S. Site-specific fluorescence reveals distinct structural changes with GABA receptor activation and antagonism. *Nat. Neurosci.* 5, 1163–1168 (2002).
24. Vilardaga, J.P., di Paolo, E. & Bollen, A. Improved PCR method for high efficacy site-directed mutagenesis using class 2S restriction enzymes. *Biotechniques* **18**, 605–606 (1995).
25. Groarke, D.A., Wilson, S., Krasel, C. & Milligan, G. Visualization of agonist-induced association and trafficking of green fluorescent protein-tagged forms of both β-arrestin-1 and the thyrotropin-realeasing hormone receptor. *J. Biol. Chem.* **274**, 23263–23269 (1999).
26. Richardson, M. & Robishaw, J.D. The α_{2A}-adrenergic receptor discriminates between G_i heterotrimers of different βγ subunit composition in Sf9 insect cell membranes. *J. Biol. Chem.* **274**, 13525–13533 (1999).

A FlAsH-based FRET approach to determine G protein–coupled receptor activation in living cells

Carsten Hoffmann[1], Guido Gaietta[2], Moritz Bünemann[1], Stephen R Adams[3], Silke Oberdorff-Maass[1], Björn Behr[1], Jean-Pierre Vilardaga[1], Roger Y Tsien[3], Mark H Ellisman[2] & Martin J Lohse[1]

Fluorescence resonance energy transfer (FRET) from cyan to yellow fluorescent proteins (CFP/YFP) is a well-established method to monitor protein-protein interactions or conformational changes of individual proteins. But protein functions can be perturbed by fusion of large tags such as CFP and YFP. Here we use G protein–coupled receptor (GPCR) activation in living cells as a model system to compare YFP with the small, membrane-permeant fluorescein derivative with two arsen-(III) substituents (fluorescein arsenical hairpin binder; FlAsH) targeted to a short tetracysteine sequence. Insertion of CFP and YFP into human adenosine A_{2A} receptors allowed us to use FRET to monitor receptor activation but eliminated coupling to adenylyl cyclase. The CFP/FlAsH-tetracysteine system gave fivefold greater agonist-induced FRET signals, similar kinetics (time constant of 66–88 ms) and perfectly normal downstream signaling. Similar results were obtained for the mouse α_{2A}-adrenergic receptor. Thus, FRET from CFP to FlAsH reports GPCR activation in living cells without disturbing receptor function and shows that the small size of the tetracysteine-biarsenical tag can be decisively advantageous.

In recent years, a large number of genetically encoded fluorescent sensors have been developed that measure protein-protein interactions or conformational changes of a protein of interest based on FRET[1]. These systems have mostly used variants of the green fluorescent protein (GFP) from *Aequorea victoria*. A problem with GFP and its derivatives is their relatively large size and hence risk of altering the properties of the labeled protein(s). For example, in fusions, CFP and YFP have altered some properties of GPCRs[2]. Agonist-induced activation of GPCRs is thought to cause a conformational rearrangement of their seven transmembrane α helices[3,4], most notably helices III and VI (refs. 3 and 5). Insertion of CFP into the third intracellular loop and fusion of YFP to the C terminus of a GPCR allows monitoring of agonist-induced activation, but impairs G protein coupling[2], as the third intracellular loop is a G protein coupling region[6,7].

Fluorescent probes for GPCR activation will be very useful for the study of the activation process and for drug screening[8]. However, the pharmacological and signaling properties of the receptor should not be disturbed by the necessary modifications. Therefore, we set out to develop an alternative approach based on FlAsH, a small fluorescent probe that we have developed for labeling of proteins in intact cells[9,10]. FlAsH is nonfluorescent by itself but becomes highly fluorescent when bound to a specific sequence consisting of at least six amino acids[9,10]. The best sequence for FlAsH binding known so far is CCPGCC[11]. FlAsH is much smaller than GFP (**Fig. 1a**), and therefore there is a much lower risk that FlAsH will disturb the overall structure of a protein.

Although FlAsH has been used for specific labeling of cellular proteins and for the study of long-term protein dynamics[10,12], no study has used FlAsH in combination with other fluorophores in dynamic FRET experiments. Here we report the use of FlAsH and CFP in dynamic FRET experiments using GPCR activation as a test system and demonstrate substantial improvements compared to the previously published CFP/YFP approach[2].

RESULTS

Generation of receptor constructs

We generated various receptor constructs based on the human A_{2A} adenosine receptor with modifications in different positions. CFP or the FlAsH-binding motif (CCPGCC) were introduced into the third intracellular loop of the receptor, and CFP or YFP were fused to its C terminus, respectively (**Fig. 1b**). Each receptor construct was fused with CFP at the same position of the C terminus. In the construct A_{2A}-CFP-Flash-C the sequence AEAAARECCPGCCARA, which binds FlAsH with high affinity[11], was fused to the C terminus of CFP. In the construct A_{2A}-Flash3-CFP, the CCPGCC sequence was in the third intracellular loop.

Specific labeling of receptor constructs with FlAsH

The specificity of FlAsH binding to the CCXXCC motif has been shown *in vitro*[9,11] and *in vivo*[10,12]. To demonstrate that FlAsH specifically binds to our receptor constructs, we transiently transfected HeLa cells with sequences encoding one of three different constructs (A_{2A}-CFP, A_{2A}-CFP-Flash-C and A_{2A}-Flash3-CFP) and incubated the cells with FlAsH. We excited the cells with two

[1]Institute of Pharmacology and Toxicology, University of Würzburg, Versbacher Str. 9, D-97078 Würzburg, Germany. [2]National Center of Microscopy and Imaging Research, Department of Neuroscience, and [3]Department of Pharmacology, University of California, San Diego, 9500 Gilman Drive, La Jolla, California 92093, USA. Correspondence should be addressed to M.J.L. (lohse@toxi.uni-wuerzburg.de).

PUBLISHED ONLINE 17 FEBRUARY 2005; DOI:10.1038/NMETH742

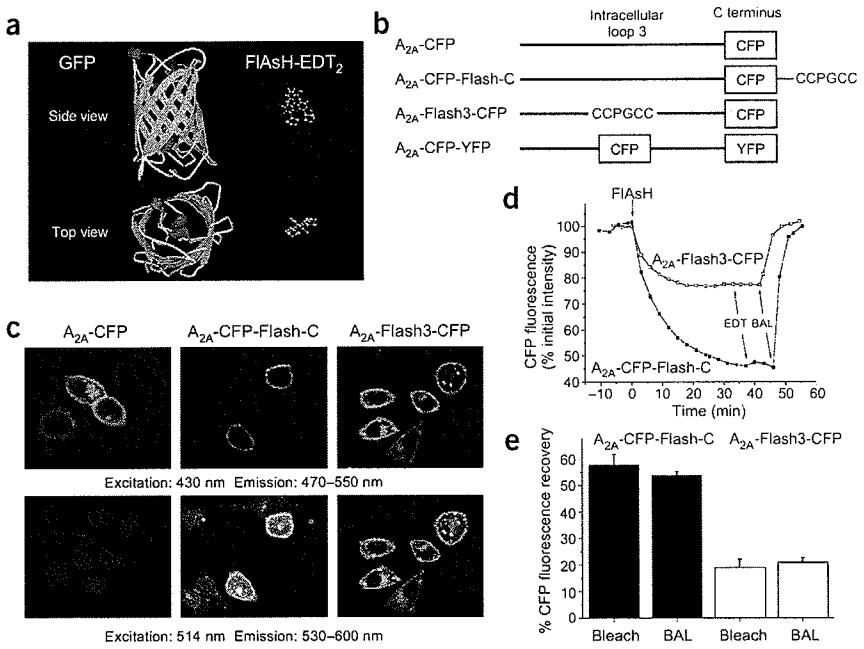

Figure 1 | Labeling of A_{2A} receptor constructs. (**a**) Size comparison of GFP (backbone only) and FlAsH-EDT_2. (**b**) Schematic representation of receptor constructs. All constructs are variants of the human A_{2A} wild-type receptor and were modified as indicated either at the C terminus, the third intracellular loop, or both locations. (**c**) Confocal microscopy images of three different receptor constructs transiently expressed in HeLa cells and labeled with FlAsH. Top, CFP fluorescence. All receptor constructs were expressed at the cell surface. Bottom, FlAsH-fluorescence. All cells show dim yellow background fluorescence owing to nonspecifically bound FlAsH, but the cells expressing constructs containing the FlAsH binding motif (center and right) show a strong yellow fluorescence at the cell surface. (**d**) FRET between CFP and FlAsH in A_{2A} adenosine receptors. HEK-293 cells transiently transfected with the construct A_{2A}-CFP-Flash-C or A_{2A}-Flash3-CFP were incubated at the indicated time point with 500 nM FlAsH. Fluorescence intensity of CFP (450–515 nm) was measured every 3 min. We added 250 μM EDT and 5 mM BAL as indicated by the arrows. (**e**) Comparison of FRET efficiency determined by fluorescence recovery after acceptor bleaching (Bleach) and after BAL treatment (BAL). Data are ±s.e.m. of 9–12 cells from three separate experiments.

different wavelengths, one specific for CFP (430 nm) and the other specific for FlAsH (514 nm), and monitored them using a confocal microscope.

Images obtained after excitation of CFP at 430 nm showed expression of the three receptor constructs at the surface of HeLa cells (**Fig. 1c**, top). Images obtained after excitation at 514 nm demonstrated specific labeling with FlAsH of only the two receptor constructs containing the FlAsH binding motif (**Fig. 1c**, bottom). In contrast, cells expressing the construct A_{2A}-CFP that cannot specifically bind FlAsH showed only dim yellow background fluorescence, demonstrating that nonspecific FlAsH labeling was low and that CFP was not fluorescent when excited at 514 nm (**Fig. 1c**, bottom). A comparison of transfected (CFP-positive) and nontransfected (CFP-negative) cells demonstrated that nonspecific FlAsH labeling amounted to about one-fifth of the specific labeling (**Fig. 1c**, bottom). These data show that the insertion of the CCPGCC motif allowed specific labeling of the receptors with FlAsH.

FRET between FlAsH and CFP

To investigate whether FRET occurred between FlAsH and CFP, we mounted cells transfected with the construct encoding A_{2A}-CFP-Flash-C or A_{2A}-Flash3-CFP on a fluorescence microscope and incubated them with 500 nM FlAsH. Progressive labeling was monitored by short (100-ms, to minimize photobleaching) excitation pulses every 3 min. A time-dependent decrease in CFP fluorescence that reached a plateau after 20–40 min was observed for both constructs (**Fig. 1d**). Further increases in FlAsH concentration did not further decrease CFP fluorescence (data not shown), indicating that labeling was complete. Washing with 250 μM 1,2-ethanedithiol (EDT) after attainment of equilibrium did not affect donor (CFP) fluorescence. But CFP fluorescence recovered when the acceptor fluorescence was eliminated by stripping FlAsH from the tetracysteine using 5 mM 2,3-dimercapto-1-propanol (BAL), a vicinal dithiol with even higher affinity for arsenicals than EDT. BAL completely dequenched the CFP fluorescence (**Fig. 1d**). This experiment allowed us to estimate the FRET efficiency at 21 ± 2% for A_{2A}-Flash3-CFP and 54 ± 3% for A_{2A}-CFP-Flash-C (**Fig. 1e**).

FRET efficiency was also measured by donor dequenching after acceptor photobleaching: we illuminated the FlAsH-labeled cells for 5 min at 514 nm to bleach FlAsH completely and measured fluorescence recovery of the donor fluorophore. The values obtained were quite similar to those determined with the BAL experiments: 19 ± 3% for A_{2A}-Flash3-CFP and 58 ± 4% for A_{2A}-CFP-Flash-C (**Fig. 1e**).

Agonist-dependent changes in FRET signals

We then investigated whether the FRET signal obtained with A_{2A}-Flash3-CFP was sensitive to agonist stimulation. HEK-293 cells transiently expressing this construct were labeled with FlAsH and then stimulated by superfusion with the agonist adenosine. This led to a symmetrical decrease of the FlAsH emission and increase of the CFP emission and thus to a rapid loss of FRET, indicated by ~10% decrease in the 535 nm/480 nm FRET ratio (**Fig. 2a**). The loss of FRET is compatible with the hypothesis that activation would lead to an increased distance between the third intracellular loop and the C terminus of GPCRs[2] as predicted by computer simulations with the α_{1B}-adrenergic receptor[7].

In contrast to A_{2A}-Flash3-CFP, the construct A_{2A}-CFP-Flash-C that has both fluorophores at the C terminus did not change fluorescence upon agonist stimulation (data not shown). Coexpression of A_{2A}-CFP and A_{2A}-Flash3 (carrying only the Flash motif in the third intracellular loop but lacking the CFP) showed no

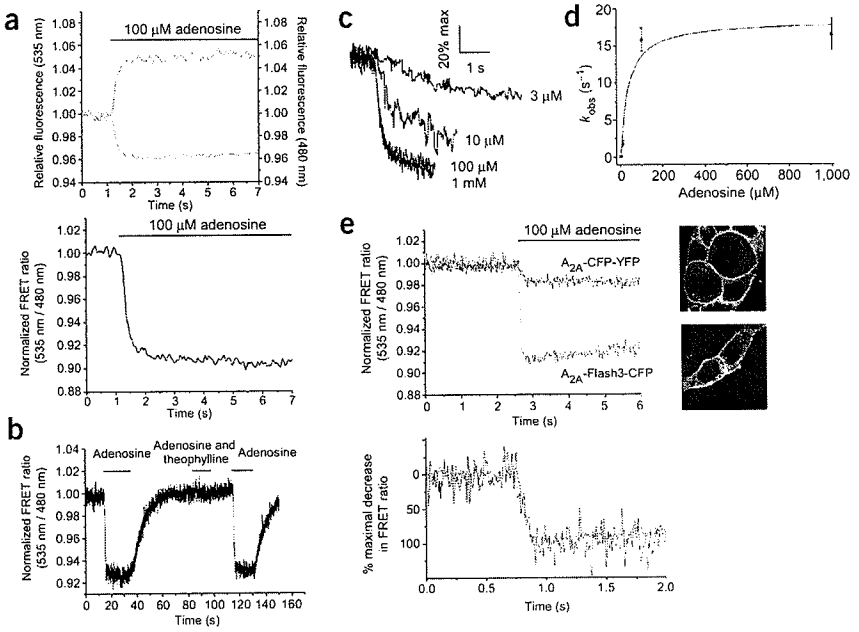

Figure 2 | Adenosine-induced changes in FRET in FlAsH/CFP-labeled A_{2A} receptors (A_{2A}-Flash3-CFP). (**a**) Changes in the relative fluorescence of CFP or FlAsH (top) and corresponding FRET ratio (bottom) in response to 100 μM adenosine from a single HEK-293 cell expressing the construct A_{2A}-Flash3-CFP. Initial values of relative fluorescence (top) or of the normalized FRET ratio (bottom) were set to one. The recording is representative of a large number of independent experiments. (**b**) Changes in the FRET ratio of A_{2A}-Flash3-CFP expressed in HEK-293 cells upon agonist stimulation and blockade by an antagonist. Superfusion was done with buffer, with (or without) 10 μM adenosine with or without 500 μM theophylline. (Representative experiment, $n = 3$). (**c**) Kinetics of adenosine-mediated change in the FRET ratio. The change in the normalized FRET ratio in response to different concentrations of the agonist adenosine measured in single cells expressing A_{2A}-Flash3-CFP. The recordings are expressed as % of the maximal response achieved with 1 mM adenosine (representative experiment, $n = 4$). (**d**) Relationship between the adenosine concentration and k_{obs}, the apparent rate constant of the change in the FRET ratio. k_{obs} values were obtained from fitting the kinetic data to a monoexponential equation. (**e**) Comparison of FRET signals in FlAsH/CFP- and in CFP/YFP-labeled receptors. Top, normalized FRET ratios in response to 1 mM adenosine from single HEK-293 cells expressing A_{2A}-Flash3-CFP (red) or A_{2A}-CFP-YFP (black). Right, confocal images of the respective receptors. Bottom, same data with the amplitude (responses to 1 mM adenosine) set to 100% for both traces.

FRET in the absence or presence of 100 μM adenosine (data not shown). These control experiments indicate that it is unlikely that the observed signals resulted from intermolecular FRET in receptor dimers. But it should be noted that the intramolecular nature of this signal does not exclude the presence of receptor dimers.

The agonist-induced change in the FRET signal of the A_{2A}-Flash3-CFP construct was blocked by an antagonist, theophylline. In consecutive stimulations of the same cell with 10 μM adenosine, a robust signal was obtained with adenosine alone, whereas no response was seen in the presence of 500 μM theophylline (**Fig. 2b**). Theophylline alone had no effect, and in accordance with the pattern expected for competitive antagonism, raising the adenosine concentration to 100 μM partially reversed the theophylline block (data not shown).

Time-resolved recordings of the FRET signals from single cells after activation with adenosine allowed the analysis of the activation switch kinetics (**Fig. 2c,d**). Under all conditions, the decrease of the FRET ratio (535 nm/480 nm) followed a mono-exponential time course. Increasing concentrations of adenosine resulted in faster time courses of the signals, until at higher concentrations the rate constants (k_{obs}) reached a maximum, suggesting that a step other than agonist binding became rate limiting. This limit is not due to technical limitations of the system, which allows complete solution exchange in < 10 ms, and therefore most likely represents (or at least includes) the agonist-mediated conformational switch of the receptors. The maximal k_{obs} values of 15–20 sec^{-1} indicate a time constant required for receptor activation of 50–70 ms.

Comparison of FlAsH/CFP with CFP/YFP-modified receptors

To compare the new labeling approach to that using CFP and YFP, we created an adenosine receptor (A_{2A}-CFP-YFP), in which CFP was inserted in the third intracellular loop at the position of the FlAsH-binding motif in A_{2A}-Flash3-CFP, and YFP was at the C terminus instead of CFP (**Fig. 1b**).

A direct comparison of the two FRET approaches shows that the amplitude of the signal for the FlAsH/CFP-modified receptor was five times higher than that of the CFP/YFP–modified receptor (**Fig. 2e**). But the time constant of receptor activation was not substantially different for the two approaches. When the two FRET signals were normalized with respect to the signal amplitude (**Fig. 2e**, bottom), the FlAsH/CFP-based approach gave a time constant of 66 ± 8 ms ($n = 7$), whereas the CFP/YFP-based approach gave a value of 88 ± 18 ms ($n = 5$). These values are close to those previously reported for the CFP/YFP-labeled α_{2A}-adrenergic receptor (~50 ms) but are much faster than for the

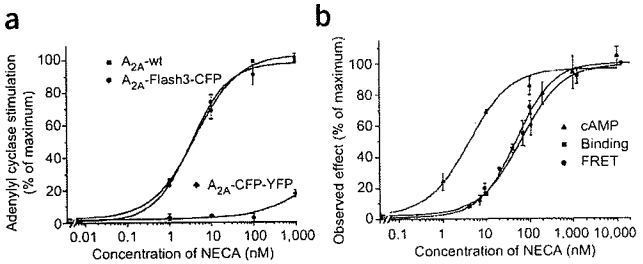

Figure 3 | Pharmacological properties of the A_{2A} receptor constructs. (**a**) Stimulation of adenylyl cyclase activity by NECA in cell membranes from HEK cells expressing A_{2A} wild-type receptors (squares), A_{2A}-Flash3-CFP (circles), or A_{2A}-CFP-YFP (diamonds). Data are ±s.e.m. ($n = 3$). (**b**) Comparison of NECA-binding (squares), NECA-induced changes in FRET (circles) and NECA-induced adenylyl cyclase stimulation (triangles) for A_{2A}-Flash3-CFP. All data are given as percent of the response induced by 1 mM NECA. Data are ±s.e.m. ($n = 3$–4).

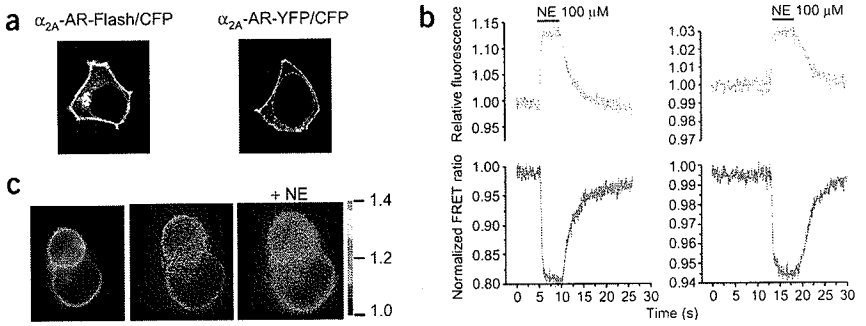

Figure 4 | Application of the FlAsH/CFP approach to the α_{2A}-adrenergic receptor. (**a**) Confocal pictures show the cellular expression of the α_{2A}-AR-Flash/CFP and α_{2A}-AR-YFP/CFP in transiently transfected HEK-293 cells. Both receptor constructs exhibit predominant localization to the plasma membrane. (**b**) Changes in the fluorescence (top) of CFP and FlAsH (left) or CFP and YFP (right), respectively and corresponding FRET-ratio (bottom) in response to 100 μM norepinephrine were recorded from a single HEK-293 cell expressing α_{2A}-AR-Flash/CFP or α_{2A}-AR-YFP/CFP. Initial values of relative fluorescence (top; blue, 480 nm and yellow, 535 nm) or of the normalized FRET ratio (bottom; red, 535 nm/480 nm) were set to one. The recording is representative of a large number of independent experiments. (**c**) FRET imaging of receptor activation in HEK-293 cell transiently transfected with α_{2A}-AR-Flash/CFP. The left panel shows fluorescence emission of the cells upon excitation at 430 nm. The next two panels show the FRET ratio presented as a false-color image (480 nm/535 nm) before and after stimulation with 100 μM norepinephrine. The scale bar on the right indicates the false-color scale of the ratios.

PTH receptor studied by the same approach ($\sim$1 sec)[2]. The signal-to-noise ratio of the FlAsH/CFP-based approach is substantially better when compared to the CFP/YFP-based approach (**Fig. 2e**).

Pharmacological characterization of receptor constructs

To investigate whether the insertion of the CCPGCC motif or GFP variants into the receptor affect the receptor's binding or signaling properties, the wild-type A_{2A} receptor, A_{2A}-Flash3-CFP and A_{2A}-CFP-YFP were each transiently expressed in COS-1 cells. All three receptors were expressed at comparable levels varying from 8 to 12 pmol/mg protein and bound the agonist radioligand [^{3}H]NECA with affinities of 52 $\pm$ 9, 63 $\pm$ 11 and 63 $\pm$ 18 nM, respectively (data not shown).

The constructs were analyzed for their signaling properties by determination of adenylyl cyclase activation upon receptor stimulation with NECA (**Fig. 3a**). The activation curves for the wild-type receptor and A_{2A}-Flash3-CFP were superimposable, suggesting that the G protein coupling and signaling properties of the receptor were not affected by these labels. In marked contrast, the receptor construct A_{2A}-CFP-YFP mediated almost no adenylyl cyclase stimulation even at high agonist concentrations.

The NECA-binding and FRET signal curves of A_{2A}-Flash3-CFP were superimposable, whereas—owing to signal amplification—the adenylyl cyclase activation curve was shifted to lower concentrations by one order of magnitude (**Fig. 3b**). This illustrates that the FRET signal faithfully records the agonist-occupied active state of the receptor rather than a downstream-mediated effect.

FlAsH/CFP labeling of α_{2A}-adrenergic receptors

To investigate whether this FlAsH/CFP approach can be applied to other systems, we constructed an α_{2A}-adrenergic Flash/CFP receptor (α_{2A}-AR-Flash/CFP) containing the CCPGCC motif instead of the YFP in the previously published α_{2A}-YFP/CFP receptor[2]. Confocal images (**Fig. 4a**) showed that even in transiently transfected HEK-293 cells both receptor constructs are primarily expressed at the plasma membrane. A typical trace of the agonist-induced change in the FRET signal is shown in **Figure 4b**. Upon superfusion with norepinephrine, the change in the FRET signal was again more than threefold greater for the FlAsH/CFP construct than for the CFP/YFP receptor and amounted to up to a 20% change. This change in signal amplitude was large enough for imaging of receptor activation in real time. We transfected HEK-293 cells with α_{2A}-AR-Flash/CFP, labeled them with FlAsH and recorded FRET images with a dual-emission CCD camera. Upon superfusion with norepinephrine, the cells showed a marked change in fluorescence ratio (**Fig. 4c**). The bar on the right shows the false-color scale of the corrected CFP/FlAsH emission. Note that in this experiment the CFP/FlAsH ratio is such that addition of agonist increases the ratio. A movie of the experiment reveals the temporal as well as the spatial resolution of our FlAsH/CFP imaging technique (**Supplementary Video 1** online).

DISCUSSION

The recently described direct monitoring of receptor activation with optical techniques opens new dimensions of temporal and spatial information on the activation of GPCRs[2,8]. But the technique based on the fusion of two GFP variants to the receptor has drawbacks owing to the large size of the fluorescent markers, which can lead to alterations in the pharmacological and signaling properties of the receptors.

Therefore, we have developed a modification of this system that replaces the fluorescent protein in the third intracellular loop of the receptor with tetracysteine-FlAsH and uses CFP at the C terminus as the fluorescence donor. This approach is the first report of dynamic FRET using FlAsH in combination with CFP to monitor conformational changes in a protein and illustrates the potential of this small fluorescent marker to label defined proteins in an intact cell. Its much smaller size compared to GFP resulted in preservation of the pharmacological properties of the A_{2A} receptor with respect both to agonist binding and to agonist-induced cAMP signaling. This is remarkable because the insertion of a fluorescent protein at the same site in this receptor (that is, the third intracellular loop) virtually abolished the signaling capacity of the receptor.

In addition to preserving the receptor's pharmacological properties, the FlAsH approach also resulted in much larger agonist-induced changes in FRET, both in the A_{2A}-adenosine and the α_{2A}-adrenergic receptor (**Figs. 2e** and **4b**). This increased signaling amplitude appeared to be a true sensing property of the FlAsH-labeled receptors, as both the FlAsH/CFP- and CFP/YFP-labeled receptors were primarily targeted to the cell surface and thus were available for agonist activation. A possible explanation is the relative distance and orientation of the two fluorophores: because

FlAsH directly binds to the CCPGCC motif, it is located directly at the third intracellular loop of the receptor, whereas in the case of the fluorescent proteins the fluorophore is located inside the β barrel ~10–15 Å away from the site of attachment in the third intracellular loop. In addition, the attachment of FlAsH at its binding site may be less flexible than that of YFP and, therefore, FlAsH may more faithfully report the conformational change.

It might be assumed that the presence of FlAsH instead of YFP would permit the receptor to switch faster in response to agonists, as the large additional protein moiety might restrain the receptor's movement. This, however, was not the case. There are two mutually nonexclusive explanations for this observation. The actual conformational change makes up only part of the k_{obs} measured for receptor activation. For example, ligand diffusion, binding to the relevant site within the receptor and the fact that we observed a multitude of receptors at the cell surface rather than a single one might all contribute to apparent switch times that are longer than the actual conformational change. Alternatively, the presence of a 27-kDa fluorescent protein in the third intracellular loop does not limit the speed of the conformational change within the receptor protein. Based on the measured translational and rotational diffusion behavior of GFP in cytoplasm[13], one can calculate that GFP by itself can undergo major rotations or a 2.5-nm lateral diffusion in only tens of nanoseconds, some six orders of magnitude less than the 66–88 ms observed for the receptor switch. Thus, a fused GFP mutant can be completely nondisruptive with respect to intrinsic conformational kinetics of the receptor, whereas it severely obstructs interaction with downstream effectors.

The improved agonist-induced FRET signal for the A_{2A}-Flash3-CFP construct enabled us to compare this signal with radioligand binding and cAMP production induced by the same ligand. The data obtained for the FRET signal are almost superimposable with those from radioligand binding (**Fig. 3b**). This would be expected if binding of an agonist directly led to a conformational change in the receptor. Thus, only agonist-occupied receptors should change their relative FRET ratio and, therefore, the signal should follow binding of the ligand. The leftward shift for the cAMP accumulation (**Fig. 3b**) relative to radioligand binding and the FRET signal probably is due to a receptor reserve: not all receptors need to be activated to generate a full cAMP signal. Furthermore, the antagonist theophylline blocked the agonist-induced change in the FRET signal (**Fig. 2b**) and did not induce a signal by itself (data not shown). This suggests that the FRET signal reflects agonist-induced receptor activation. An interesting feature of the FlAsH-labeled receptors is the greater amplitude of the agonist-induced FRET signal. This should allow more detailed analysis of the properties of compounds that only partially activate receptors, as seen for the β_2-adrenergic receptor using purified receptors and a different fluorescence labeling system[14] and the α_{2A}-AR-CFP/YFP system[2]. In particular, it will be interesting to determine whether the existence of several distinct agonist-induced states, which have recently been determined for the β_2-adrenergic receptor[14,15], also holds for other GPCRs, and to delineate whether FRET signals can be used to distinguish between these states. This potential of our new technology will have to be thoroughly investigated in the future. Another potential application of this technique is outlined in **Figure 4c**. The amplitude of the signal change for the α_{2A}-AR-Flash/CFP construct was large enough to use the receptor construct for imaging of receptor activation in real time. This experiment indicates that this technique can be applied to visualize receptor activation in other relevant physiological models.

Taken together, the use of FlAsH as a label in conjunction with CFP improves detection of GPCR activation at the single cell level. We believe that the use of this approach will substantially advance both the analysis of the mechanisms of receptor activation and the use of optical methods in ligand screening. Although the small size of the tetracysteine-biarsenical tagging system has long been theoretically attractive, this example is the first direct demonstration of a major reduction in perturbation of host protein function.

METHODS

Molecular biology and cell culture. Site-directed mutagenesis was performed on the human adenosine A_{2A} receptor cDNA (GenBank entry X68486). The cDNAs encoding the enhanced CFP and YFP were fused to the receptor cDNA such that the fluorescent protein would follow position Gly340 or Val323 of the receptor's C terminus. CFP or the CCPGCC motif were also substituted for the sequence from Pro215 to Arg220 in the third intracellular loop of the receptor. A similar α_{2A}-AR-Flash/CFP construct was obtained by fusion at position Val461 with CFP, and the CCPGCC motif was inserted in the third intracellular loop between Ala250 and Ser371. Constructions were performed by PCR of the cDNA and verified by sequencing. Receptor cDNAs were cloned into pcDNA3 (Invitrogen) for expression in HeLa, HEK-293 and COS-1 cells. COS-1 cells were transfected using DEAE-Dextran[16], and Effectene (Qiagen) was used for HEK-293 and HeLa cells. For fluorescence measurements, cells were split 24 h after transfection and seeded on polylysine-coated coverslips that were placed in six-well plates. Cells were kept in culture for an additional 24 h. For live-labeling experiments and the determination of FRET efficiency, cells were cultured on 3-cm MatTek dishes (MatTek Corporation).

FlAsH labeling. The labeling was done essentially as described[10]. Transfected cells grown on coverslips or MatTek dishes were washed twice with phenol red–free Hank's balanced salt solution containing 1g/l glucose (HBSS; Invitrogen) and then incubated at 37 °C for 1 h with 500 nM or 1 μM FlAsH suspended in HBSS containing 12.5 μM EDT. Next, cells were rinsed twice with HBSS, incubated for 10 min with HBSS containing 250 μM EDT and again rinsed twice with HBSS to reduce nonspecific labeling. FlAsH is commercially available from Invitrogen as Lumino Green.

Confocal microscopy. Confocal microscopy was performed using a Leica TCS SP2 system with an Attofluor holder (Molecular Probes). FlAsH was excited with the 514-nm line of an argon laser, and images were taken with a 63× objective using the factory settings for YFP fluorescence (530–600 nm). CFP was excited at 430 nm with a frequency-doubled diode laser (Leica) and images were taken using the factory settings for CFP fluorescence (470–550 nm).

Live labeling and determination of FRET efficiency. HEK-293 cells cultured in 3-cm MatTek dishes were transiently transfected as described above. After 24 h, cells were washed twice with phenol red–free HBSS and maintained in 1.9 ml HBSS buffer. MatTek

dishes were mounted on a Zeiss Axiovert135 inverted fluorescence microscope and measured using MetaFluor software. The following excitation/dichroic/emission filters were used: for CFP, 420 ± 20 nm/450 nm/475 ± 40 nm; for FlAsH, 495 ± 10 nm/505 nm/535 ± 25 nm; and for FRET between CFP and FlAsH, 420 ± 20 nm/450 nm/535 ± 25 nm. Light pulses were of 100-ms duration. To monitor labeling, regions of interest were defined and a time drive was set to take pictures with the above settings every 3 min. After 10 min, 100 µl of a freshly prepared mix of FlAsH dye and EDT was added to a final concentration of 500 nM FlAsH and 12.5 µM EDT. Fluorescence emission was monitored until a plateau was reached. Next, the incubation mixture was aspirated carefully, ensuring that no movement of the specimen occurred; cells were incubated with HBSS supplemented with 250 µM EDT; and fluorescence emission was monitored every 3 min. After 10 min, the incubation mixture was carefully aspirated and cells were incubated with HBSS. FRET between CFP and FlAsH was then quantified by two different methods: (i) treatment with BAL to compete for FlAsH binding and (ii) donor dequenching after acceptor photobleaching (5-min illumination at 495 nm).

Fluorescence measurements and cell imaging. Fluorescence microscopy was performed as described[2,17]. Cells labeled as described above were washed with HBSS and maintained in buffer A (140 mM NaCl, 5 mM KCl, 2 mM $CaCl_2$, 1 mM $MgCl_2$, 10 mM HEPES, pH 7.3) at room temperature. Coverslips were mounted on an Attofluor holder and placed on a Zeiss Axiovert135 inverted microscope equipped with an oil immersion 63× objective and a dual emission photometric system (Till Photonics). Samples were excited with light from a polychrome IV (Till Photonics). To minimize photobleaching, the illumination time was set to 5 ms, applied with a frequency between 1 and 100 Hz depending on agonist concentration. The fluorescence signal was recorded from the entire cell. FRET was monitored as the emission ratio of FlAsH to CFP, F_{535}/F_{480} (emission intensities at 535 ± 15 nm and 480 ± 20 nm; beam splitter DCLP 505 nm) upon excitation at 436 ± 10 nm (beam splitter DCLP 460 nm). The emission ratio was corrected for the spillover of CFP into the 535 nm channel (spillover of FlAsH into the 480 nm channel was negligible) to give a corrected ratio (F^*_{535}/F^*_{480}). The FlAsH emission upon excitation at 480 nm was recorded at the beginning of each experiment to subtract direct excitation of FlAsH (FlAsH emission at 436 nm excitation divided by FlAsH emission at 480 nm excitation was 0.06). To determine agonist-induced changes in FRET, cells were continuously superfused with buffer A, and agonist was applied using a computer-assisted solenoid valve–controlled rapid superfusion device ALA-VM8 (ALA Scientific Instruments; solution exchange 5–10 ms). Signals detected by avalanche photodiodes were digitized using an AD converter (Digidata1322A, Axon Instruments) and stored on PC using Clampex 8.1 software (Axon Instruments). The decrease in FRET ratio (r) was fitted to the equation $r(t) = A \times e^{-t/\tau}$, where τ is the time constant (s) and A is the magnitude of the signal. When necessary for calculating τ, agonist-independent changes in FRET owing to photobleaching were subtracted. The imaging data were recorded as previously described[18]. Data were analyzed with MetaMorph 5.0 (Visitron Systems).

Pharmacology. Membrane preparation, ligand binding and determination of adenylyl cyclase activity were performed as previously described[19]. Saturation and competition binding studies were analyzed with the program Origin (OriginLab Corporation) to calculate K_D and K_i values.

Note: Supplementary information is available on the Nature Methods website.

ACKNOWLEDGMENTS

This work was supported by the Deutsche Forschungsgemeinschaft (Leibniz award to M.J.L. and grant HO 2357/1-1 to C.H.), a Bavaria California Technology Center (BaCaTeC) grant to C.H., a Fonds der Chemischen Industrie grant to M.J.L. and US National Institutes of Health grant P41RR004050 to M.H.E.

COMPETING INTERESTS STATEMENT

The authors declare competing financial interests (see the *Nature Methods* website for details).

Received 14 October 2004; accepted 26 January 2005
Published online at http://www.nature.com/naturemethods/

1. Miyawaki, A. Visualization of the spatial and temporal dynamics of intracellular signaling. *Dev. Cell* **4**, 295–305 (2003).
2. Vilardaga, J.P., Bünemann, M., Krasel, C., Castro, M. & Lohse, M.J. Measurement of the millisecond activation switch of G protein-coupled receptors in living cells. *Nat. Biotechnol.* **21**, 807–812 (2003).
3. Gether, U. Uncovering molecular mechanisms involved in activation of G protein-coupled receptors. *Endocr. Rev.* **21**, 90–113 (2000).
4. Pierce, K.L., Premont, R.T. & Lefkowitz, R.J. Seven-transmembrane receptors. *Nat. Rev. Mol. Cell Biol.* **3**, 639–650 (2002).
5. Bissantz, C. Conformational changes of G protein-coupled receptors during their activation by agonist binding. *J. Recept. Signal Transduct. Res.* **23**, 123–153 (2003).
6. Wess, J. G-protein-coupled receptors: molecular mechanisms involved in receptor activation and selectivity of G-protein recognition. *FASEB J.* **11**, 346–354 (1997).
7. Greasley, P.J. *et al.* Mutational and computational analysis of the alpha(1b)-adrenergic receptor. Involvement of basic and hydrophobic residues in receptor activation and G protein coupling. *J. Biol. Chem.* **276**, 46485–46494 (2001).
8. Milligan, G. Applications of bioluminescence- and fluorescence resonance energy transfer to drug discovery at G protein-coupled receptors. *Eur. J. Pharm. Sci.* **21**, 397–405 (2004).
9. Griffin, B.A., Adams, S.R. & Tsien, R.Y. Specific covalent labeling of recombinant protein molecules inside live cells. *Science* **281**, 269–272 (1998).
10. Gaietta, G. *et al.* Multicolor and electron microscopic imaging of connexin trafficking. *Science* **296**, 503–507 (2002).
11. Adams, S.R. *et al.* New biarsenical ligands and tetracysteine motifs for protein labeling in vitro and in vivo: synthesis and biological applications. *J. Am. Chem. Soc.* **124**, 6063–6076 (2002).
12. Ju, W. *et al.* Activity-dependent regulation of dendritic synthesis and trafficking of AMPA receptors. *Nat. Neurosci.* **7**, 244–253 (2004).
13. Swaminathan, R., Hoang, C.P. & Verkman, A.S. Photobleaching recovery and anisotropy decay of green fluorescent protein GFP-S65T in solution and cells: cytoplasmic viscosity probed by green fluorescent protein translational and rotational diffusion. *Biophys. J.* **72**, 1900–1907 (1997).
14. Swaminath, G. *et al.* Sequential binding of agonists to the β2 adrenoceptor. Kinetic evidence for intermediate conformational states. *J. Biol. Chem.* **279**, 686–691 (2004).
15. Liapakis, G., Chan, W.C., Papadokostaki, M. & Javitch, J.A. Synergistic contributions of the functional groups of epinephrine to its affinity and efficacy at the beta2 adrenergic receptor. *Mol. Pharmacol.* **65**, 1181–1190 (2004).
16. Cullen, B.R. Use of eukaryotic expression technology in the functional analysis of cloned genes. *Methods Enzymol.* **152**, 684–704 (1987).
17. Bünemann, M., Frank, M. & Lohse, M.J. Gi protein activation in intact cells involves subunit rearrangement rather than dissociation. *Proc. Natl. Acad. Sci. USA* **100**, 16077–16082 (2003).
18. Nikolaev, V.O., Bünemann, M., Hein, L., Hannawacker, A. & Lohse, M.J. Novel single chain cAMP sensors for receptor-induced signal propagation. *J. Biol. Chem.* **279**, 37215–37218 (2004).
19. Klotz, K.N. *et al.* Comparative pharmacology of human adenosine receptor subtypes—characterization of stably transfected receptors in CHO cells. *Naunyn Schmiedebergs Arch. Pharmacol.* **357**, 1–9 (1998).